# Numerical modeling of dam-break flood flows for dry and wet sloped beds

Mostafa Bigdeli[1*], Mercedeh Taheri[1,2], Abdolmajid Mohammadian[1]

1) Department of Civil Engineering, University of Ottawa, Ottawa, Ontario K1N6N5, Canada

2) School of Civil Engineering, College of Engineering, University of Tehran, Tehran, Iran

* Corresponding author: mbigd068@uottawa.ca

## Abstract

Investigation of the effects of sloping dry and wet immobile beds on downstream dam-break flows is of great importance given the destructive power of these flows. Such investigation can lead to the adoption of appropriate measures and timely control strategies. In this study, numerical simulations of experimental wave propagation were carried out using four models, i.e., $k-\omega$-SST-RANS, realizable $k-\varepsilon$-RANS, Smagorinsky-LES, and $k-\omega$-SST-DES on sloped beds, for the first time as its novelty, with respect to upstream water and different downstream tail-water depths. The $k-\omega$-SST-DES exhibited the best performance in the simulation of wave peak patterns and mean velocities. Taylor diagrams showed that all models were similar in estimating the highest R values and lowest centered root-mean-square errors for dry beds. However, for wet beds with higher downstream tail-water depths, the CRMSE were higher. For lower depths, the standard deviations of the models were generally closer to those of the flume experimental measurements conducted by Liu et al. (2020). The present study has shed light on the levels of turbulence models' accuracy in simulation of dam-break flows on dry and wet sloping beds, and can be taken as a basis for further understanding of the flood flow behavior in future studies.

**Keywords**: Upstream, Downstream, Dam-break flow, Tail-water, Sloping bed

## 1. Introduction

Dam-breaks pose a risk for serious environmental crises, as powerful and destructive dam-break floods not only have significant effects downstream but can also lead to considerable loss of life (Hamlet and Lettenmaier, 2007; Liu et al., 2020; Plate, 2002; Wang et al., 2020b). More than 40 dam failures have been reported since the year 2000 over the world which have led to irreparable damage to both human life and ecosystems (Li and Zhao, 2018). Many of these dams reportedly failed when a sudden break created a flood wave that propagated and emitted a large volume of water, particles, or both into a horizontal or inclined channel within a short time (i.e., time to failure). There are also several known examples of water-reserving or earth-filling tailings dams collapsing. The failure of the Vajont dam in Italy killed 1,910 individuals in 1963 because of the reservoir overflowing, and the failure of the Situ Gintung dam in Indonesia took the lives of 100 people in 2009. In addition, the collapse of a tailings dam in Myanmar in 2015 killed no less than 113 people, while in Mariana, Brazil, a tailings dam collapse in 2015 claimed at least 17 lives, with its slurry wave polluting more than 15 $km^2$ of surrounding land and waterways (Li and Zhao, 2018). Since dam-breaks can cause catastrophic events on downstream floodplains, dam and flood control structures are very important (Chanson, 2006b). These structures improve the safety of water storage and enable dams to be exploited for several purposes, such as flood control, water supply, electricity generation, etc. by controlling water levels (Biegowski et al., 2020; Novák et al., 2007). Hence, understanding dam-break flood characteristics in order to diminish the risk of flood occurrence and save lives is vital. In other words, accurate determination of dam-break flood arrival times, its maximum levels, and depths is a worthwhile endeavor in order to minimize catastrophic flood consequences and provide noticeable improvements in emergency readiness.

Many experimental and numerical studies have addressed the dam-break process (Bell et al., 1992; Bellos et al., 1992; Dressler, 1954; Lauber and Hager, 1998; Mohsenabadi et al., 2019), and experimental research on dam breaks and flood waves has been conducted since the late 20th century (Bell et al., 1992; Bellos et al., 1992; Dressler, 1954; Fraccarollo and Toro, 1995; Lauber and Hager, 1998; Vosoughi et al., 2020). Free-water surface variation measurements with regard to the times of dam-break incidents have been mainly included in experimental modeling of dam-break flows (Ismail et al., 2020; Miller and Hanif Chaudhry, 1989; Schmidgall and Strange,

1960), with many previous experimental studies addressing the issue in different initial conditions including dry-bed or wet-bed downstream for a fixed channel bed (Frazão and Zech, 2002; Bellos, 2004; Yang et al., 2011; Kocaman and Ozmen-Cagatay, 2012; LaRocque et al., 2013; Meile et al., 2013; Ozmen-Cagatay et al., 2014; Wood and Wang, 2015; Vosoughi et al., 2020). In addition, theoretical solutions for dry- and wet-bed conditions were derived in the 1800s (Ritter, 1892; Li and Zhao, 2018;). An unlimited length for both reservoirs and channels was assumed in early theoretical solutions (Ismail et al., 2020; Ritter, 1892) for a dam-break event. Ritter's (1892) solution was further developed by Stoker (1957) by solving Saint-Venant equations in order to relate wet-bed and dry-bed conditions downstream of a dam by using the method of characteristics. Method of characteristics is a numerical solution method for certain type of equations such as shallow water equations. In this method, the equations are decomposed along the characteristic curves which make them simplified and ready to solve by standard numerical methods. Solutions for dam-break propagation on sloped beds were reported later (Chanson, 2006a; Ismail et al., 2020); however, the proposed analytical solutions were not compatible with experimental data, especially during the initial phases of a dam break (Mohsenabadi et al., 2019; Ozmen-Cagatay and Kocaman, 2010; Stansby et al., 1998). With this in mind, more studies should be performed to describe actual dam-break flows.

Indeed, the value of using dam-break problems for the verification of mathematical and physical methods has been noted in the scientific community (Li and Zhao, 2018; Wang et al., 2000). Considerable numerical studies on dam-break phenomena were conducted in the late $20^{th}$ century by using computational fluid dynamics (CFDs) to assess 1D and 2D dam breaks (Beam and Warming, 1976; Beljadid et al., 2016; Gabutti, 1983; Ghazizadeh et al., 2019; Liu et al., 2017; Mingham and Causon, 1998; Mohammadian et al., 2007; Shirkhani et al., 2016). Reynolds-averaged Navier-Stokes (RANS) models can describe unsteady-state problems such as dam-break flows. These RANS equations have been solved using the finite difference method so that the free surface was captured by using the volume of fluid (VOF) (Shigematsu et al., 2004). A Eulerian finite volume method (FVM) was used in a Navier-Stokes solver in order to simulate the dam break problem by Abdolmaleki et al. (2004). To measure the quantity of the flood wave propagation, two different approaches, i.e., the finite volume method (FVM) and the finite element method (FEM), have been compared in dam-break modeling (Quecedo et al., 2005).

As stated above, numerical dam-break research has focused on more complicated cases including wet-bed downstream conditions (Aliparast, 2009; Crespo et al., 2008; Wu and Wang, 2007). Most of these studies have reported varied factors that affect a dam-break flow, although the bed slope and the depth of the tail-water downstream play important roles compared with other factors in the formation of dam-break flows (Feizi Khankandi et al., 2012; Hooshyaripor and Tahershamsi, 2015; Juez et al., 2017; Miller and Hanif Chaudhry, 1989; Van Emelen et al., 2014; Wang et al., 2018). Recognizing the features of dam-break flows on sloping dry or wet beds can lead to the provision of flood alerts and the adoption of timely appropriate measures. In this respect, numerous studies have assessed dam-break flows on sloping beds. Elliptic integrals have been used to determine solutions for dam-break flood propagation over a sloped dry bed (Dressler, 1958), and a mathematical equation was developed and used for a sloped dry bed case to depict water surface profiles (Mungkasi and Roberts, 2010). Different analytical solutions based on various approaches have also been derived (Fernandez-Feria, 2006; Mangeney et al., 2000). Besides the effect of sloping beds on a dam-break flow, the downstream water depth (i.e., tail-water depth) also affects this type of flow. A dynamic wave estimation was applied by Hunt (1983) to obtain the analytical solution for dam-break flows on a wet sloped bed, while a similar study was conducted for shallow water to obtain the analytical solution for wet sloped beds (Wang et al., 2020a). Given that there have been few studies on dam-break flows on sloped wet beds, the propagation aspects of dam-break flows on these beds have remained somewhat unknown. Therefore, in the current study, we address the effects of dam-break flood flows on the water surface and its velocity at downstream of the proposed flume, particularly to investigate such effects on slope wet beds. This is a novelty of this paper since we simulated dam-break flood flows on sloping beds for the first time by using different CFD turbulence models.

This study aims to simulate dam-break flows on sloping wet and dry beds by using OPEN Field Operation And Manipulation (OpenFOAM) with various turbulence models. The profiles of flow parameters such as free water surface and mean velocity were tracked and extracted for each slope for different downstream tail-water depths, and the results from the current numerical study were compared with the results of the recent experimental study by Liu et al. (2020).

## 2. Methodology, formulation, and numerical models

One useful tool used in many numerical studies for the fluid phase is CFD, which can solve a locally averaged Navier-Stokes equation (Anderson and Jackson, 1967; Li and Zhao, 2018). In this study, CFD was employed to simulate the tail-water downstream of a dam break. A free open-source software package, OpenFOAM, was adopted for the CFD modules (Weller et al., 1998). OpenFOAM is a C++ toolbox which is available for different operating system platforms and has been used in several previous hydraulic engineering studies (Kheirkhah Gildeh et al., 2016; Mohsenabadi et al., 2019; Shaheed et al., 2019). OpenFOAM can simulate a fluid stream since it can be customized for numerical problems (e.g., fluid flows in channels, wind tunnel tests, heat transfer, etc.) and turbulence models. The toolbox has two major abilities: solving particular fluid mechanics problems by its solvers, and manipulating data through its utilities. OpenFOAM can be used for both time intervals and space integration using FVM. In this study, interFoam was employed, which is a solver used for incompressible, isothermal immiscible turbulent flows, and uses the volume of fluid method.

### 2.1. Governing equations for turbulent flows

In this study, the three-dimensional RANS equations that include continuity and momentum for incompressible flows are provided as follows (Holzmann, 2017; Imanian and Mohammadian, 2019):

$$\nabla . U = 0 \tag{1}$$

$$\frac{\partial \rho U}{\partial t} + \nabla . (\rho UU) = \nabla . \tau + \rho g - \nabla p \tag{2}$$

where $\nabla$ is nabla (gradient operator), U is the flow velocity vector, $\rho$ is the fluid density, t is time, $\tau$ is the shear-rate (viscous stresses) tensor, g is the gravitational acceleration vector, and $p$ is the pressure.

## 2.2. Turbulence Models

In this study, dam-break flows were simulated for the first time on sloped beds by using four precise turbulence models: the $k-\omega$-SST-RANS (RANS), realizable $k-\varepsilon$ (RANS), Smagorinsky (LES), and $k-\omega$-SST-DES (DES). The methods are described below. To increase the accuracy of the results and the reality of the simulations, a mixture of RANS, Large Eddy Simulation (LES), and Detached Eddy Simulation (DES) models was employed.

### 2.2.1. RANS Models

#### 2.2.1.1. $k-\omega$-SST-RANS

The standard $k-\omega$ model uses shear flow spreading, compressibility, and low-Reynolds number effects modifications, while the $k-\omega$-SST (Shear Stress Transport) model is an extension of the standard $k-\omega$ model. The model estimates adverse pressure gradients, separating flows, and turbulence behavior when they are not in local equilibrium (Imanian and Mohammadian, 2019). $k$ and $\omega$ are defined through solving the equations below in the $k-\omega$-SST model (Lee, 2018):

$$\frac{\partial k}{\partial t}+u_i\frac{\partial k}{\partial x_i}=\frac{\partial}{\partial x_i}\left[(\nu+\sigma_k\nu_T)\frac{\partial k}{\partial x_i}\right]+P_k-\beta^* k\omega \tag{3}$$

$$\frac{\partial \omega}{\partial t}+u_i\frac{\partial \omega}{\partial x_i}=\frac{\partial}{\partial x_i}\left[(\nu+\sigma_\omega\nu_T)\frac{\partial \omega}{\partial x_i}\right]+\alpha S^2-\beta\omega^2+2(1-F_1)\sigma_{\omega 2}\frac{1}{\omega}\frac{\partial k}{\partial x_j}\frac{\partial \omega}{\partial x_j} \tag{4}$$

where $u$ indicates velocity, $P_k=\min(G,10\beta^* k\omega)$ with $G=\nu_T\nabla u:[\nabla u+(\nabla u)^T]$, $S=\sqrt{2D:D}$ with $D=[\nabla u+(\nabla u)^T]/2$, $F_1$ represents a blending function, ":" indicates the multiplication of tensors, and $\beta^*$, $\sigma_k, \alpha, \beta, \sigma_\omega,$ and $\sigma_{\omega 2}$ are model coefficients. The turbulent viscosity, $\nu_T$, is defined as follows (Lee, 2018):

$$\nu_T=min\left(\frac{k}{\omega},\frac{a_1 k}{\Omega F_2}\right) \tag{5}$$

where $F_2$ is determined based on the distance to the wall, $a_1$ is a constant, and $\Omega=|[\nabla u-(\nabla u)^T]/2|$. $F_2=1$ and $F_2=0$ in the inner and the outer layers, respectively. $F_1$and $F_2$ fall off to zero well within the inner layer and at the edge, respectively.

2.2.1.2. Realizable $k-\varepsilon$

The realizable $k-\varepsilon$ model is the latest version of the $k-\varepsilon$ model (Cable, 2009; Shih et al., 1995). The model has two major differences in comparison with the standard $k-\varepsilon$ model. First, the turbulent viscosity is presented in the improved formulation, and second, the equation for the dissipation rate is provided through the mean-square vorticity transport equation (Shih et al., 1995; Wang and Wang, 2011). Flow features such as strong streamline curvature, vortices, and rotation are addressed in the realizable $k-\varepsilon$ model more precisely (Wang and Wang, 2011). Therefore, the realizable $k-\varepsilon$ model predicts the characteristics of separated or complex secondary flows more accurately (Cable, 2009; Wang and Wang, 2011). Among all the $k-\varepsilon$ model versions, the realizable $k-\varepsilon$ model provides the best performance in predicting the dissipation rates of flat distribution and round jets (Bulat and Bulat, 2013). The improved transport equations are shown below (Shih et al., 1995):

$$\frac{\partial}{\partial t}(\rho k)+\frac{\partial}{\partial x_j}(\rho k u_j)=\frac{\partial}{\partial x_j}\left[\left(\mu+\frac{\mu_t}{\sigma_k}\right)\frac{\partial k}{\partial x_j}\right]+G_k+G_b-\rho\varepsilon-Y_M+S_K \quad (6)$$

$$\frac{\partial}{\partial t}(\rho\varepsilon)+\frac{\partial}{\partial x_j}(\rho\varepsilon u_j)=\frac{\partial}{\partial x_j}\left[\left(\mu+\frac{\mu_t}{\sigma_\varepsilon}\right)\frac{\partial \varepsilon}{\partial x_j}\right]+\rho C_1 S\varepsilon-\rho C_2\frac{\varepsilon^2}{k+\sqrt{\nu\varepsilon}}+C_{1\varepsilon}\frac{\varepsilon}{k}C_{3\varepsilon}G_b+S_\varepsilon \quad (7)$$

where $G_b$ represents turbulent kinetic energy generation increases due to buoyancy, and $Y_M$ is the fluctuating dilation incompressible turbulence influencing the overall dissipation rate. $S_\varepsilon$ and $S_K$ represent source terms provided by the user, and $\sigma_k$ and $\sigma_\varepsilon$ indicate the turbulent Prandtl numbers for the turbulent kinetic energy and its dissipation.

2.2.2. LES Model

2.2.2.1. Smagorinsky

The eddy viscosity can be predicted by the Smagorinsky model so that in regions of intense shear such as near-solid boundaries, it reaches the highest values. The Smagorinsky model, as one of the most popular sub-grid scale (SGS) models, directly connects the deviatoric part of the SGS stress tensor $\left(\tau_{ij}^D=\tau_{ij}-\tau_{kk}\delta_{ij}/3\right)$ to the resolved strain rate tensor $\left(\overline{S_{ij}}\right)$ (Montazerin et al., 2015):

$$\tau_{ij}^{D,Smag} = -2\nu_t^{Smag}\overline{S_{ij}} \quad (8)$$

where the Smagorinsky eddy viscosity ($\nu_t^{Smag}$) and $\overline{S_{ij}}$ are defined as follows:

$$\nu_t^{Smag} = \left(C_{Smag}\Delta\right)^2|\bar{S}| \quad (9)$$

$$\overline{S_{ij}} = \frac{1}{2}\left(\frac{\partial\overline{u_i}}{\partial x_i} + \frac{\partial\overline{u_j}}{\partial x_j}\right) \quad (10)$$

Strain magnitude, $|\bar{S}| = \sqrt{2\overline{S_{ij}S_{ij}}}$, indicates the characteristic filtered strain rate, and $C_{Smag}$ represents the Smagorinsky coefficient. The Smagorinsky model is popularly used for major reasons such as being simple to implement and that it behaves well in numerical solutions. Compared to other SGS models, the Smagorinsky model yields a more accurate prediction of SGS stress due to the accordance of the Smagorinsky coefficient to the local flow behavior (Montazerin et al., 2015).

### 2.2.3. DES Model

#### 2.2.3.1. $k-\omega$-SST-DES

The $k-\omega$-SST-DES model is an improved version of the $k-\omega$-SST model (Lindblad et al., 2014; Menter et al., 2003), and since it is a low Reynolds number model, it is not necessary for the $k-\omega$ model to include extra damping functions to ensure accurate behavior close to walls. In order to reduce turbulent viscosity in regions with fine mesh, the model was equipped with DES features. By employing the DES features, the model shifts from RANS mode to LES mode effectively in such regions so that turbulent viscosity should be considered as sub-grid-scale viscosity. The $\omega$ value can be shown as a ratio of $k$ to $\varepsilon$:

$$\omega = \frac{\varepsilon}{\beta^* k}\ ,\ \beta^* = C_\mu \quad (11)$$

where $C_\mu$ is the constant that indicates the turbulent viscosity in the $k-\varepsilon$ model, and is equal to 0.09. The $k-\omega$-SST-DES model uses the modeled transport equation for the turbulent kinetic energy, $k$, as follows (Davidson, 2006; Menter et al., 2003):

$$\frac{\partial k}{\partial t} + \frac{\partial (\overline{u_i} k)}{\partial x_i} = \widetilde{P_k} + \frac{\partial}{\partial x_i}\left[\left(\nu + \frac{\nu_t}{\sigma_k}\right)\frac{\partial k}{\partial x_i}\right] - \beta^* k\omega F_{DES} \quad (12)$$

Terms $F_{DES}$ and $\widetilde{P_k}$, which are modified production variables, make this transport equation different from similar equations in the base models. Since u represents the turbulence, the bar over the velocity indicates that not all turbulent fluctuations are resolved in the velocity field. The subsequent transport equation considers ω as below (Davidson, 2006; Menter et al., 2003):

$$\frac{\partial \omega}{\partial t} + \frac{\partial (\overline{u_i} \omega)}{\partial x_i} = P_\omega + \frac{\partial}{\partial x_i}\left[\left(\nu + \frac{\nu_t}{\sigma_\omega}\right)\frac{\partial \omega}{\partial x_i}\right] - \beta\omega^2 + 2(1 - F_1)\sigma_{\omega^2}\frac{1}{\omega}\frac{\partial k}{\partial x_i}\frac{\partial \omega}{\partial x_i} \quad (13)$$

where the production term in the ω equation is defined as (Lindblad et al., 2014):

$$P_\omega = \alpha S^2 \quad (14)$$

As stated above, the term $S = \sqrt{2\overline{s_{iJ}}\overline{s_{iJ}}}$ indicates the invariant measure of the strain rate.

## 2.3. Numerical Model Setup and Mesh Sensitivity

A rectangular flume with dimensions of 18 m long, 1.0 m wide, and 1.09 m high was modeled to conduct the numerical study, as shown in Fig. 1. The VOF was divided into two parts as an initial condition similar to the experimental study (Liu et al., 2020). The reservoir's volume was defined as 8.37 m long, 1.0 m wide, and 0.4 m high ($h_u$), and the downstream tail-water was adjusted for dry and wet beds using different initial heights ($h_d$) equal to 0, 0.12, 0.20, and 0.28 m. Along with a zero sloped bed, two beds with slopes equal to 0.003 and 0.02 were modeled considering the mentioned initial conditions. A sensitivity analysis was carried out to investigate the influence of the mesh size, and accordingly, a mesh of fixed rectangular cells using Cartesian coordinates was considered as the computational domain. The computational domain was constructed with square cells of size Δx=Δy=13 mm through a Cartesian cell-centered discretization. Seven grid sizes of 5, 10, 11, 13, 15, 16, and 20 mm with an expansion ratio of 1:2 were analyzed to determine the optimum mesh size. Since no significant differences were seen between the wave-fronts under grid sizes higher than 13 mm, a grid size of 13 mm was adopted in both directions to reduce the computational efforts. The number of cells in the x and y directions was 1350 and 82, respectively, and was the same for all the turbulence models. The

mesh system encompassed 110,700 cells in total for all turbulence models. All surfaces of the channel were assumed to be hydraulically smooth. The upstream boundary, downstream boundary (for the wet-bed tests), lower boundary, and side-walls were set as walls, given no inflow and constant reservoir length. For the dry-bed cases, the downstream boundary was chosen as the outflow. Constant atmospheric pressure and zero shear stress were considered as boundary conditions to account for air-water interaction (Hirt and Nichols, 1981).

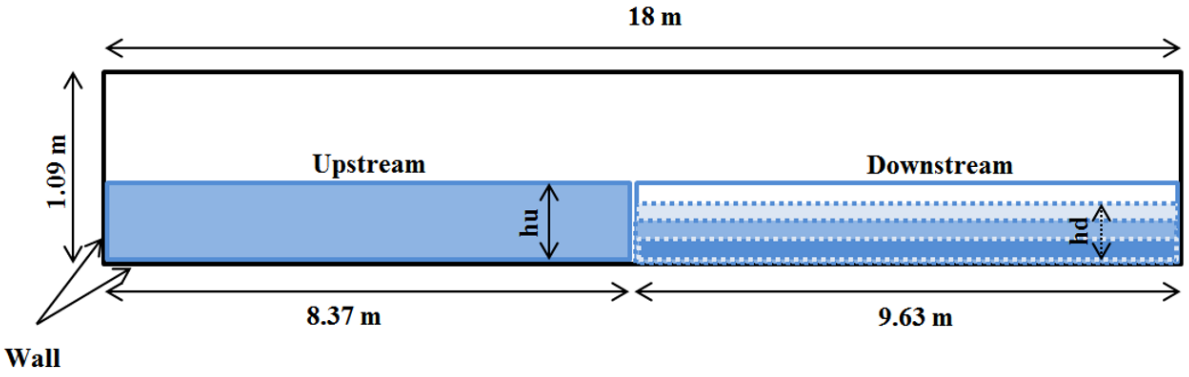


**Figure 1- 2D scheme of zero-sloped bed numerical model setup and boundary conditions**

## 3. Results and Discussion

### 3.1. Hydraulic parameters

In order to compare the results of the current numerical study with the experimental results, the hydraulic parameters are defined as follows (Liu et al., 2020):

$$Z = \frac{z}{h_u} \tag{15}$$

$$T = \frac{t}{\sqrt{h_u/g}} \tag{16}$$

$$U = \frac{u}{\sqrt{g h_u}} \tag{17}$$

where z, t, and u indicate the water level, time, and mean velocity, respectively, and Z, T, and U are the corresponding dimensionless parameters.

### 3.2. Comparative Analysis

A qualitative comparison was implemented between the results of the current study models and the experiments (Fig. 2). The different evolution patterns of the dam-break flow at t = 0.42 s for flat (Fig. 2(a)), mild (Fig. 2(b)), and steep bed slopes (Fig. 2(c)) were assessed for dry and wet bed conditions. Reasonable agreement is observed in Fig. 2 between the simulations by almost all the turbulence models and the experimental results. The wave-front resistance affected the flow more for slopes equal to 0 and 0.003 and caused higher water depths due to the absence of a significant slope effect. Unlike mild slopes, a considerable increase in the gravity component due to a steep slope in the flow direction led to the formation of thinner wave-fronts (Liu et al., 2020). The water surface warped upward for all three bed slopes during the interaction of the inflow and tail-water downstream. Moreover, the CPU times for executing the RANS, LES, and DES models were approximately 500, 600, and 900 seconds respectively. Thus, the RANS approach is preferable to the others for large computational domains in terms of lower CPU time. It should be noted that in order to make a clear comparison between the experimental measurements and the numerical results and to investigate the accuracy of different turbulence models in predicting the front wave behavior, the experimental values of Liu et al. (2020) are presented in Figs 3-6.

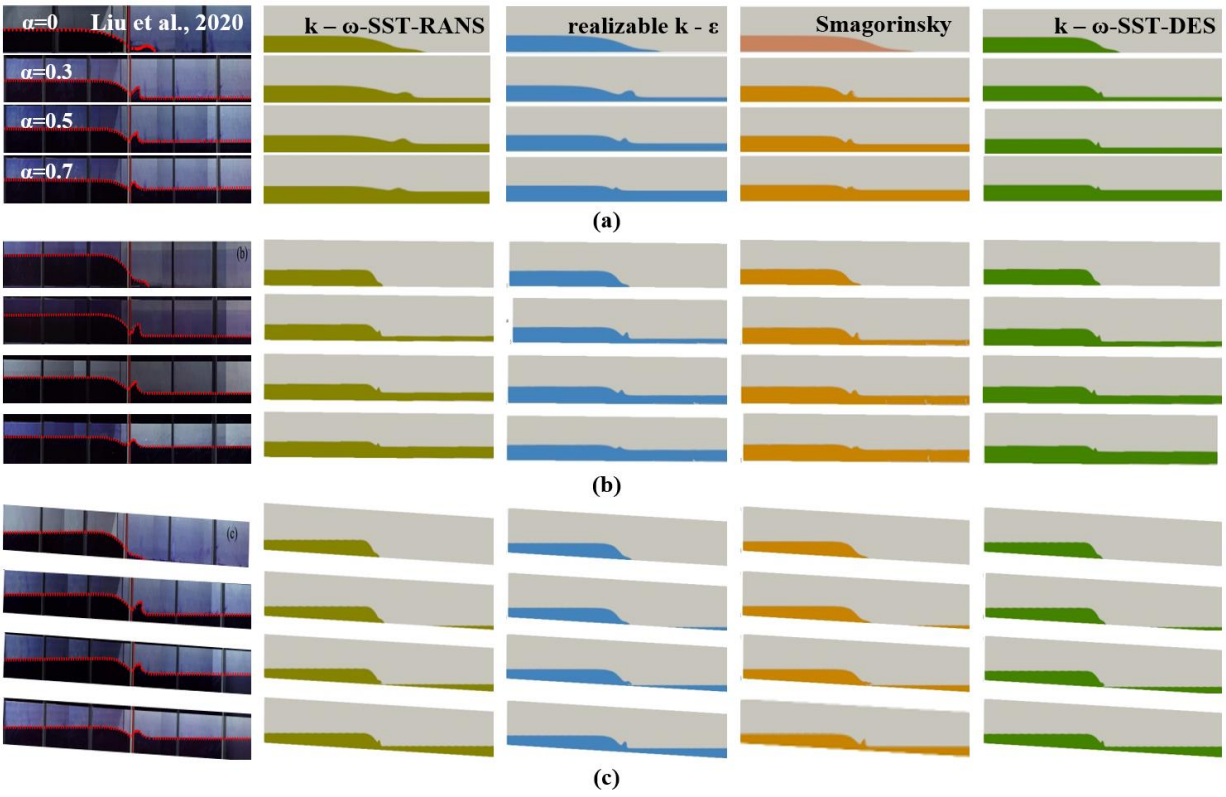


**Figure 2- Evolution pattern of the dam-break flows at t = 0.42 s (a) S = 0; (b) S = 0.003; (c) S = 0.02**

### 3.3. Water surface profile

The water level variations are shown in Fig. 3 for all three slopes for both the dry- and wet-bed channels. The different water depth ratios were defined as $\alpha = h_d/h_u$. There is good general agreement for the surface profiles between the experimental measurements (Liu et al., 2020) and the numerical estimations for T=4.95 and 9.9, especially as the flood wave moves downstream along the channel. All the turbulence models simulated the dimensionless water depth and the position of the downstream wave-front more accurately for slope=0.02. The resistance effect on the wave-front zone is the major difference between the experimental and numerical results for the dry bed condition (i.e. $\alpha = 0$), as shown in Fig. 3(a). For the wet-bed scenarios, Figs. 3(b), 3(c), and 3(d) show the upward warp that occurred at T=4.95 and 9.9 for $\alpha = 0.3$, 0.5, and 0.7 respectively. Among the sloping beds, all the models except for $k-\omega$-SST-RANS agreed well with the experimental results for slope=0.02 for $\alpha = 0.3$ and 0.7 at both T=4.95 and 9.9. There was also little difference between the numerical and experimental dimensionless water levels for the other two bed slopes, even though the $k-\omega$-SST-DES model showed the best performance

in capturing the wave peak patterns. It can be seen that the simulated water level was generally lower than the one measured at T=4.95 for S = 0 and 0.003 during the evolution process when $\alpha = 0.5$, while different results were obtained at T=9.9. In both the reservoir area and downstream of the dam, the periodic waves were predicted by the turbulence models when α increased to 0.7, which was the same as in the experimental results. Moreover, to compare the precision and the efficiency of the RANS and DES models, the results of two turbulence models, i.e., $k-\omega$-SST-RANS and $k-\omega$-SST-DES, were assessed. The $k-\omega$-SST-DES model had better performance for all slopes with different α. It can be concluded that the DES model is more capable in simulating the downstream wave-front behavior than the RANS model.

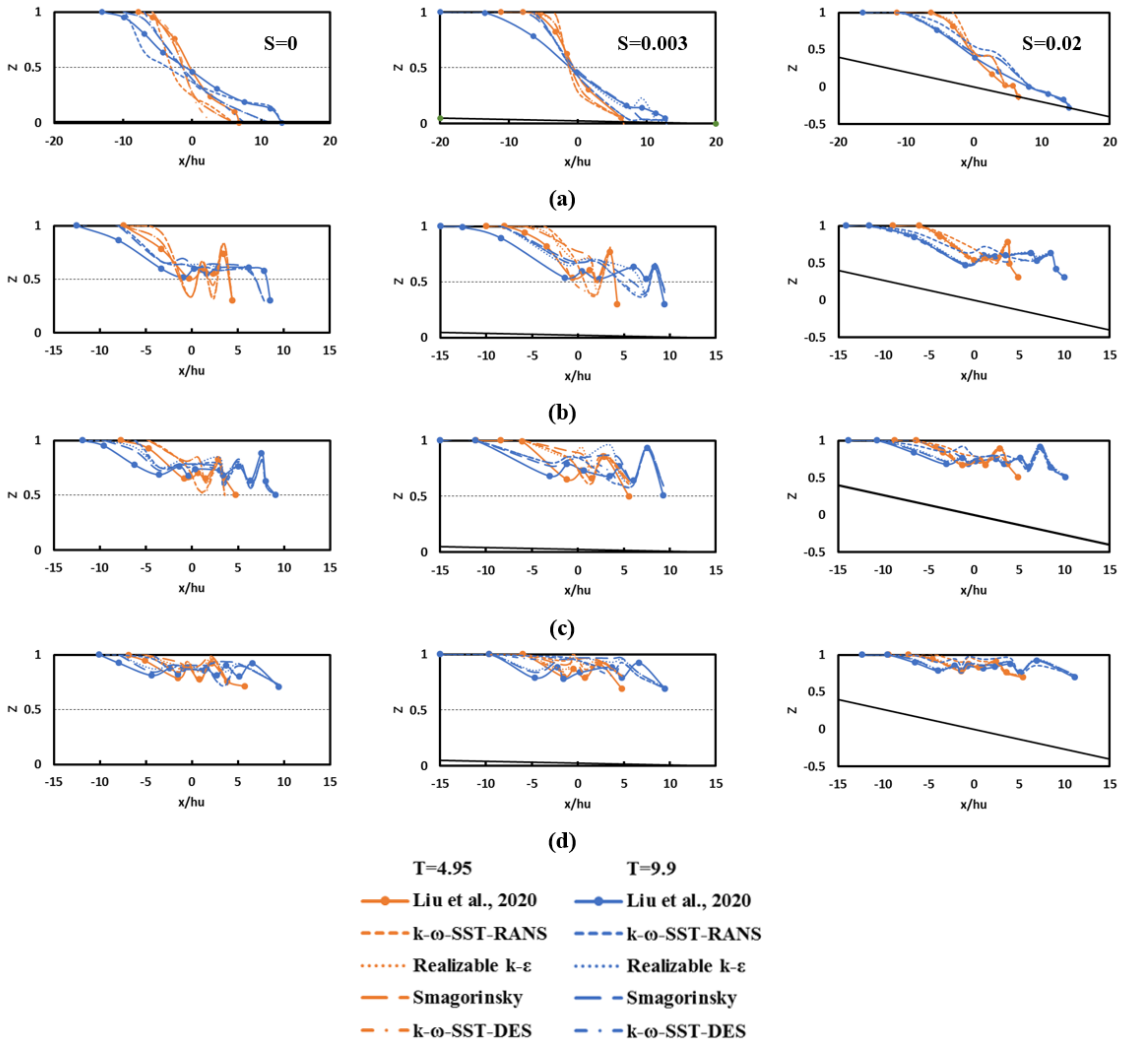


**Figure 3- Dimensionless free surface profiles for (a) α = 0; (b) α = 0.3; (c) α = 0.5; (d) α = 0.7**

306 3.4. Mean velocity profile

307 The dimensionless mean velocity profiles of the flat, mild, and steep beds under different
308 conditions (dry or wet) downstream are shown in Fig. 4 at both T=4.95 and 9.9. The numerical
309 estimations were in good general agreement with the experimental measurements (Liu et al.,
310 2020). The velocity of the flow on the dry bed increased as time progressed, and the maximum
311 velocity occurred in the downstream wave-front (Fig. 4 (a)), while it was not obtained at the
312 downstream of the wet beds (with different α values). In other words, the flow velocity slowly
313 increased and had a sudden drop downstream of the dam in the dry bed condition. All four
314 turbulence models predicted the flow velocity well when the dry-bed slope was equal to 0.003 at
315 T=4.95 and 9.9 in comparison with the other slopes, for which the flow velocities were
316 underestimated. However, for wet-bed slopes equal to 0 and 0.003, the flow velocities were
317 clearly under- and overestimated respectively. The peak became closer to the reservoir area when
318 the downstream water depth reached α = 0.3 (Fig. 4(b)). Unlike the good agreement between the
319 simulated and experimental flow velocities for the steep slope when $\alpha = 0.3$, as shown in Figs.
320 4(c) and 4(d), the distribution velocity had wave fluctuations in both the upstream and
321 downstream zones for α = 0.5 and 0.7. It was seen that the numerical results, excluding the $k -$
322 $\omega$-SST-RANS estimations, agreed well with the experimental data for slopes equal to 0 and 0.02.
323 Among the turbulence models, the $k - \omega$-SST-DES model showed slightly better performance
324 in simulating the flow velocity, which indicates the higher capability of the DES model
325 compared with the RANS model.

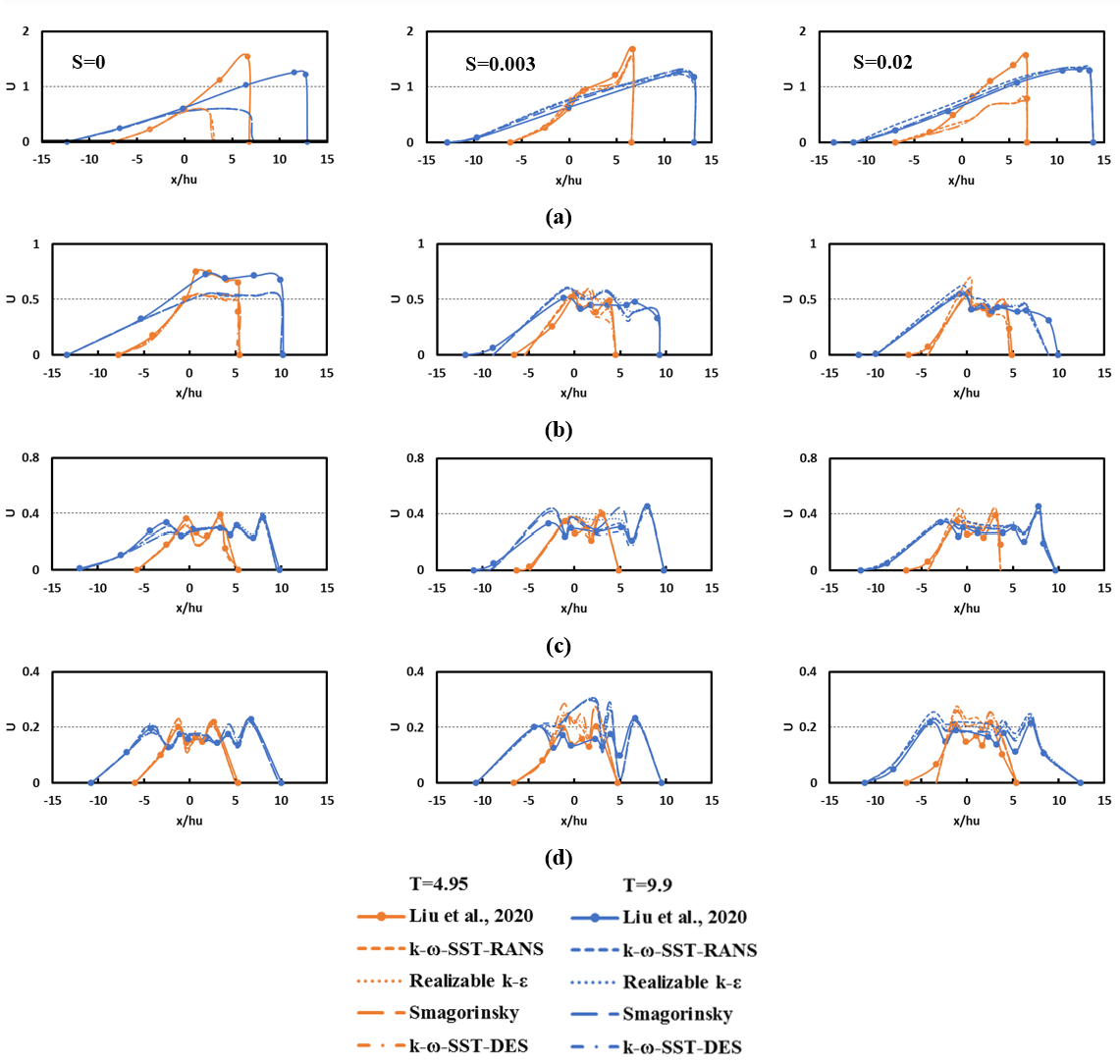


**Figure 4- Dimensionless mean velocity profiles for (a) α = 0; (b) α = 0.3; (c) α = 0.5; (d) α = 0.7**

## 3.5. Statistical analysis

The statistical parameters can be used to find the best models in terms of performance. In order to perform a statistical evaluation to assess the models' efficiency in simulating the water levels and mean velocities from the experimental results, the turbulence models were compared using three widely used statistical indicators: correlation coefficient (R), centered root-mean-square error (CRMSE), and standard deviation (SD), as shown below (Taheri et al., 2020):

$$R = \frac{cov(X_i^{expr}, X_i^{calc})}{\sqrt{var(X_i^{expr}) \times var(X_i^{calc})}} \quad (18)$$

$$CRMSE = \sqrt{\frac{\sum_{i=1}^{n}\left((X_i^{calc} - X_{mean}^{calc}) - (X_i^{expr} - X_{mean}^{expr})\right)^2}{n}} \quad (19)$$

$$SD = \sqrt{\frac{\sum(X_i - X_{mean})^2}{n}} \quad (20)$$

where $X_i^{calc}$ and $X_i^{expr}$ are the calculated and experimental hydraulic parameters values, respectively, and n represents the population of points. A larger value for R corresponds to a better linear performance of a model. Unlike R, for smaller CRMSE, the model's accuracy is higher. This is because it measures the differences of the standard deviations of $X_i^{calc}$ and $X_i^{expr}$. The most accurate simulations are related to the closest numerical standard deviations compared to the experimental ones.

In this study, Taylor diagrams, as shown in Figs. 5 and 6, were provided for the free surface and mean velocity respectively. The diagrams are employed to compare the simulations of the numerical models and to understand the similarity, dissimilarity, and variance of the estimated results comprehensively using R, CRMSE, and SD simultaneously (Taylor, 2001). According to Fig. 5, it can be seen that 3 out of the four turbulence models (i.e. realizable $k-\varepsilon$, Smagorinsky, and $k-\omega$-SST-DES) had their best performance at both T=4.95 and 9.9. For all the dry bed slopes, the numerical simulations had the highest R and the least CRMSE when $\alpha = 0$. However, as α increased with the wet beds, the value of CRMSE became larger, which implies that all the turbulence models performed poorly with higher downstream tail-water depths. It is seen that the SDs of the turbulence models were generally closer to the experimental measurements with smaller α. The simulated effects of flat, mild, and steep slopes on dam-break flows are shown in Figs. 5(a), 5(b), and 5(c), respectively, and it can be seen that 3 out of the 4 turbulence models had lower CRMSE and higher R values for different downstream conditions when the slope equaled 0.02 compared to the other two slopes. The statistical results that were closest to the experimental values were obtained for the steep slope at T=9.9, including the highest R, the lowest CRMSE, and the closest SD. The Taylor diagrams of the simulated mean velocities are shown in Fig. 6. The performance of the four turbulence models was better for non-zero sloped beds at both T=4.95 and 9.9. Among the different downstream conditions, the turbulence simulations yielded the highest R and lowest CRMSE when α = 0 for the sloping beds, except

when the slope equaled 0. The closest SDs were achieved with larger α, while the models' errors in estimating the mean velocity rose as α increased for the sloped beds, as shown in Figs. 6(a), 6(b), and 6(c), in which it can be seen that 3 out of the 4 turbulence models had higher R values and lower CRMSE when the slope was equal to 0.02 in the dry and wet beds as compared to the other two slopes. The highest R, the lowest CRMSE, and numerical data SDs closest to the experimental SDs were obtained for the mild and steep slopes at T=9.9.

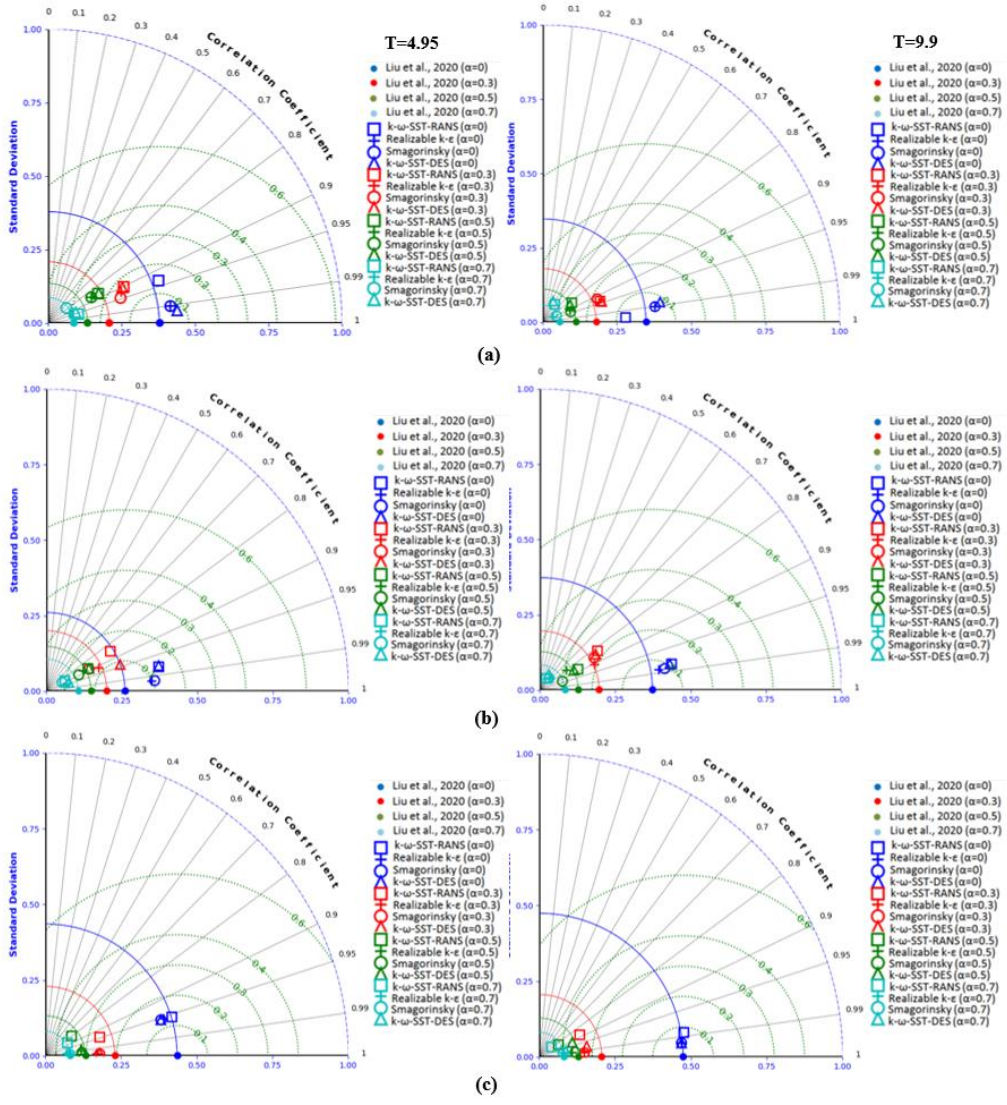


**Figure 5- Taylor diagrams for free surface estimations by k − ω-SST-RANS, realizable k − ε, Smagorinsky, k − ω-SST-DES models for (a) S = 0; (b) S = 0.003; (c) S = 0.02 vs. experiment (Liu et al., 2020) (blue, SD; green, CRMSE; black, R)**

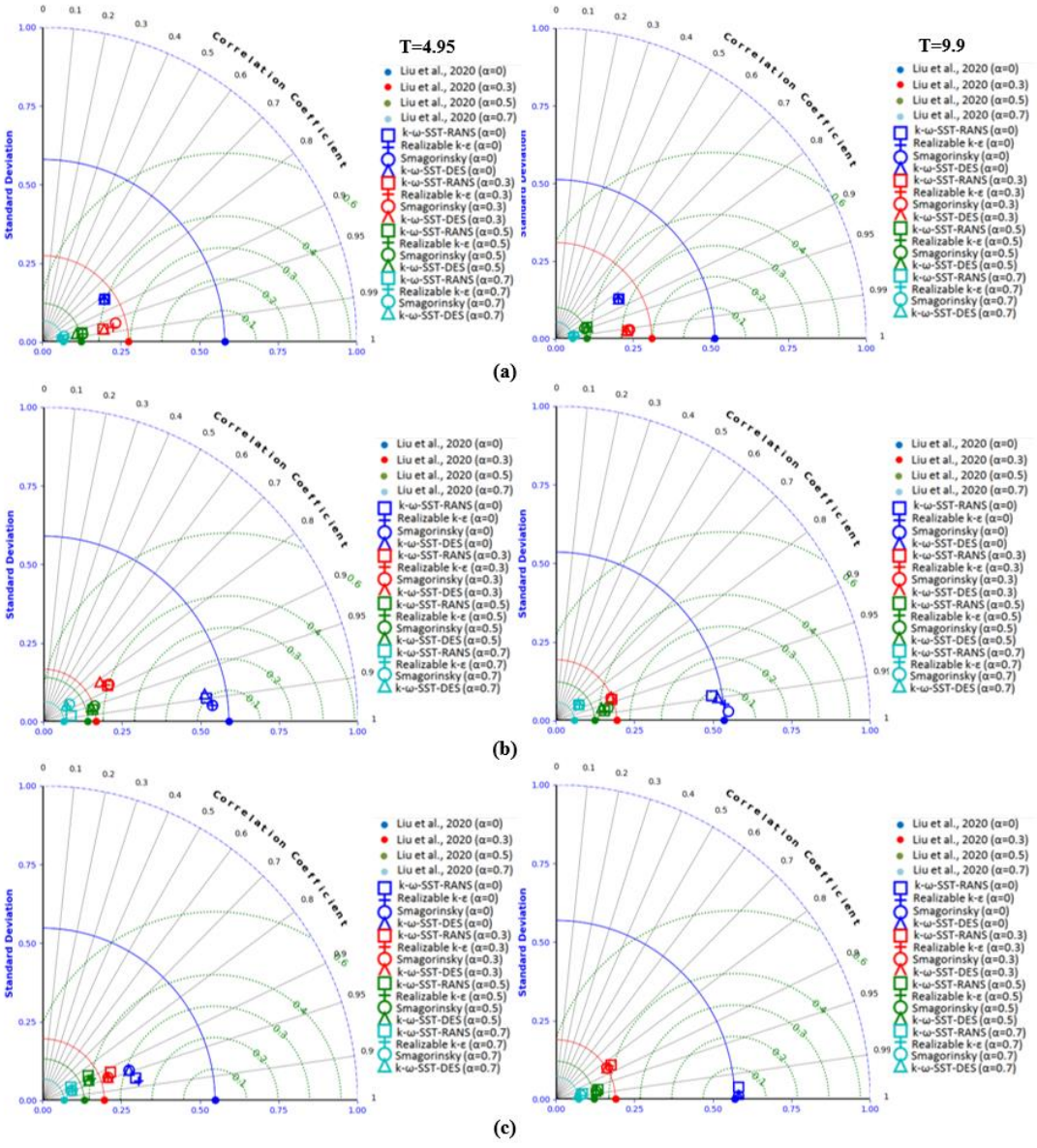


**Figure 6- Taylor diagrams for mean velocity estimations by k − ω-SST-RANS, realizable k − ε, Smagorinsky, k − ω-SST-DES models for (a) S = 0; (b) S = 0.003; (c) S = 0.02 vs. experiment (Liu et al., 2020) (blue, SD; green, CRMSE; black, R)**

Dam-break flood wave characteristics are not often similar because of different channel slopes and downstream conditions, and different outcomes can be expected in the presence of tail-water in comparison with dry beds given the perpendicular shear stresses and other dissimilarities in flood wave propagation. In addition, the existence of sloping beds affects flood flows downstream, so turbulence models might perform differently in simulating these flows. Therefore, it is necessary to determine the effects of sloping dry and wet beds on downstream

conditions. In order to reach a comprehensive understanding of flood flow behaviors with higher levels of accuracy, further studies are suggested to be conducted using various precise RANS, LES, and DES turbulence models along with different wall functions. Spending more time on assessing the evolution process of flood flow propagation is proposed for future studies.

## 4. Conclusion

In this paper, a mixture of four widely used turbulence models, i.e., $k-\omega$-SST-RANS, realizable $k-\varepsilon$, Smagorinsky, and $k-\omega$-SST-DES, were employed to simulate the results of dam-break flows for sloped dry and wet beds for the first time. The resistance effect on the wave-front zone was the major difference between the numerical results and the experimental measurements for the dry bed condition (i.e. $\alpha = 0$). For the wet-bed scenarios, figures showed that the upward warp occurred at both T=4.95 and 9.9 for $\alpha = 0.3$, 0.5, and 0.7 similar to the experimental results. Unlike the wet beds, the maximum value of the flow velocity on the dry bed was obtained in the downstream wave-front. For wet-beds (with different α values), the flow velocities were under- or overestimated. On the other hand, the free surface and mean velocity profiles of flood waves were simulated for each slope under different downstream conditions, and there were small differences between the numerical and experimental results. Some concluding remarks for the current study are summarized below:

- All models except for the $k-\omega$-SST-RANS model agreed well with the experimental results for slope=0.02. The $k-\omega$-SST-DES model showed better performance in capturing the wave peak patterns compared to the other models, especially the $k-\omega$-SST-RANS model. As well, the DES model simulated the downstream wave-fronts more accurately than the RANS model.
- All turbulence models predicted the flow velocity fairly well, especially for slope=0.02. Among the turbulence models, the $k-\omega$-SST-DES model better simulated the mean velocity.
- The highest R and the lowest CRMSE were obtained on the dry bed (i.e., α= 0). The CRMSE became larger (i.e., worse) as downstream tail-water depths increase, especially in Taylor

diagrams for free surface estimations. The SDs of the turbulence models were generally closer to that of the experimental measurements for smaller α.

- The statistical analysis led to the conclusion that 3 out of the 4 turbulence models (see Figs. 5 and 6) provided lower CRMSE and higher R values under different downstream conditions for the steep slope as compared to the other two slopes.

This study can be reckoned as a reliable reference for the simulation of ongoing and upcoming water supply projects given the obtained results and their wide applications in various environmental and engineering topics, for instance in designing hydraulic structures against tsunamis and storm surges. In addition, the results and methods can be noted in the designing phase of different types of dams on sloping beds, particularly in flood plain areas. On the other hand, more in-depth investigations are proposed including the assessments of the physical features of complex flood flows for future studies in order to reach a comprehensive understanding of the behavior of dam-break flood flows on dry and wet sloping beds with higher levels of accuracy by employing various precise RANS, LES, and DES turbulence models along with different wall functions.

## 5. References


Abdolmaleki, K., Thiagarajan, K., Morris-Thomas, M., 2004. Simulation of the dam break problem and impact flows using a Navier-Stokes solver. Simulation 13, 17.

Aliparast, M., 2009. Two-dimensional finite volume method for dam-break flow simulation. International Journal of Sediment Research 24, 99-107.

Anderson, T.B., Jackson, R., 1967. Fluid mechanical description of fluidized beds. Equations of motion. Industrial & Engineering Chemistry Fundamentals 6, 527-539.

Beam, R.M., Warming, R.F., 1976. An implicit finite-difference algorithm for hyperbolic systems in conservation-law form. Journal of computational physics 22, 87-110.

Beljadid, A., Mohammadian, A., Kurganov, A., 2016. Well-balanced positivity preserving cell-vertex central-upwind scheme for shallow water flows. Computers & Fluids 136, 193-206.

Bell, S.W., Elliot, R.C., Hanif Chaudhry, M., 1992. Experimental results of two-dimensional dam-break flows. Journal of Hydraulic Research 30, 225-252.

Bellos, C., 2004. Experimental measurements of flood wave created by a dam break. European Water 7, 3-15.

Bellos, C., Soulis, V., Sakkas, J., 1992. Experimental investigation of two-dimensional dam-break induced flows. Journal of Hydraulic Research 30, 47-63.

Biegowski, J., Paprota, M., Sulisz, W., 2020. Particle Image Velocimetry Measurements of Flow Over an Ogee-Type Weir in a Hydraulic Flume. International Journal of Civil Engineering 18, 1451-1462.

Bulat, M.P., Bulat, P.V., 2013. Comparison of turbulence models in the calculation of supersonic separated flows. World Applied Sciences Journal 27, 1263-1266.

Cable, M., 2009. An evaluation of turbulence models for the numerical study of forced and natural convective flow in Atria. Queen's University.

Chanson, H., 2006a. Analytical solutions of laminar and turbulent dam break wave, River Flow 2006: Proc., Int. Conf. on Fluvial Hydraulics, Taylor and Francis, London, pp. 465-474.

Chanson, H., 2006b. Tsunami surges on dry coastal plains: Application of dam break wave equations. Coastal engineering journal 48, 355-370.

Crespo, A., Gómez-Gesteira, M., Dalrymple, R.A., 2008. Modeling dam break behavior over a wet bed by a SPH technique. Journal of waterway, port, coastal, and ocean engineering 134, 313-320.

Davidson, L., 2006. Evaluation of the SST-SAS model: channel flow, asymmetric diffuser and axi-symmetric hill, ECCOMAS CFD. Citeseer, pp. 1-20.

Dressler, R.F., 1954. Comparison of theories and experiments for the hydraulic dam-break wave. Int. Assoc. Sci. Hydrology 3, 319-328.

Dressler, R.F., 1958. Unsteady non-linear waves in sloping channels. Proceedings of the Royal Society of London. Series A. Mathematical and Physical Sciences 247, 186-198.

Feizi Khankandi, A., Tahershamsi, A., Soares-Frazão, S., 2012. Experimental investigation of reservoir geometry effect on dam-break flow. Journal of Hydraulic Research 50, 376-387.

Fernandez-Feria, R., 2006. Dam-break flow for arbitrary slopes of the bottom. Journal of engineering mathematics 54, 319-331.

Fraccarollo, L., Toro, E.F., 1995. Experimental and numerical assessment of the shallow water model for two-dimensional dam-break type problems. Journal of hydraulic research 33, 843-864.

Frazão, S.S., Zech, Y., 2002. Dam break in channels with 90 bend. Journal of Hydraulic Engineering 128, 956-968.

Gabutti, B., 1983. On two upwind finite-difference schemes for hyperbolic equations in non-conservative form. Computers & Fluids 11, 207-230.

Ghazizadeh, M.A., Mohammadian, A., Kurganov, A., 2019. An adaptive well-balanced positivity preserving scheme on quadtree grids for shallow water equations. arXiv preprint arXiv:1911.12002.

Hamlet, A.F., Lettenmaier, D.P., 2007. Effects of 20th century warming and climate variability on flood risk in the western US. Water Resources Research 43.

Hirt, C.W., Nichols, B.D., 1981. Volume of fluid (VOF) method for the dynamics of free boundaries. Journal of computational physics 39, 201-225.

Holzmann, T., 2017. Mathematics, Numerics, Derivations and OpenFOAM (R), Holzmann CFD. Leoben, Austria. Retrieved from www. holzmann-cfd. de.

Hooshyaripor, F., Tahershamsi, A., 2015. Effect of reservoir side slopes on dam-break flood waves. Engineering Applications of Computational Fluid Mechanics 9, 458-468.

Hunt, B., 1983. Asymptotic solution for dam break on sloping channel. Journal of hydraulic engineering 109, 1698-1706.

Imanian, H., Mohammadian, A., 2019. Numerical simulation of flow over ogee crested spillways under high hydraulic head ratio. Engineering Applications of Computational Fluid Mechanics 13, 983-1000.

Ismail, H., Ann Larocque, L., Bastianon, E., Hanif Chaudhry, M., Imran, J., 2020. Propagation of tributary dam-break flows through a channel junction. Journal of Hydraulic Research, 1-10.

Juez, C., Soares-Frazao, S., Murillo, J., García-Navarro, P., 2017. Experimental and numerical simulation of bed load transport over steep slopes. Journal of Hydraulic Research 55, 455-469.

Kheirkhah Gildeh, H., Mohammadian, A., Nistor, I., Qiblawey, H., Yan, X., 2016. CFD modeling and analysis of the behavior of 30 and 45 inclined dense jets–new numerical insights. Journal of Applied Water Engineering and Research 4, 112-127.

Kocaman, S., Ozmen-Cagatay, H., 2012. The effect of lateral channel contraction on dam break flows: Laboratory experiment. Journal of hydrology 432, 145-153.

LaRocque, L.A., Imran, J., Chaudhry, M.H., 2013. Experimental and numerical investigations of two-dimensional dam-break flows. Journal of Hydraulic Engineering 139, 569-579.

Lauber, G., Hager, W.H., 1998. Experiments to dambreak wave: Horizontal channel. Journal of Hydraulic research 36, 291-307.

Lee, C. H., 2018. Rough boundary treatment method for the shear-stress transport k-ω model. Engineering Applications of Computational Fluid Mechanics, 12(1), 261-269.

Li, X., Zhao, J., 2018. Dam-break of mixtures consisting of non-Newtonian liquids and granular particles. Powder Technology 338, 493-505.

Lindblad, D., Jareteg, A., Petit, O., 2014. Implementation and run-time mesh refinement for the k− ω SST DES turbulence model when applied to airfoils. Project work. Chalmers University of Technology.

Liu, W., Wang, B., Guo, Y., Zhang, J., Chen, Y., 2020. Experimental investigation on the effects of bed slope and tailwater on dam-break flows. Journal of Hydrology 590, 125256.

Liu, X., Mohammadian, A., Sedano, J.Á.I., Kurganov, A., 2017. Three-dimensional shallow water system: A relaxation approach. Journal of Computational Physics 333, 160-179.

Mangeney, A., Heinrich, P., Roche, R., 2000. Analytical solution for testing debris avalanche numerical models. Pure and Applied Geophysics 157, 1081-1096.

Meile, T., Boillat, J.-L., Schleiss, A.J., 2013. Propagation of surge waves in channels with large-scale bank roughness. Journal of hydraulic research 51, 195-202.

Menter, F.R., Kuntz, M., Langtry, R., 2003. Ten years of industrial experience with the SST turbulence model. Turbulence, heat and mass transfer 4, 625-632.

Miller, S., Hanif Chaudhry, M., 1989. Dam-break flows in curved channel. Journal of Hydraulic Engineering 115, 1465-1478.

Mingham, C., Causon, D., 1998. High-resolution finite-volume method for shallow water flows. Journal of hydraulic engineering 124, 605-614.

Mohammadian, A., Le Roux, D., Tajrishi, M., 2007. A conservative extension of the method of characteristics for 1-D shallow flows. Applied mathematical modelling 31, 332-348.

Mohsenabadi, S.E., Mohammadian, M., Nistor, I., Gildeh, H.K., 2019. CFD modelling of near-field dam break flow, Sustainable and Safe Dams Around the World/Un monde de barrages durables et sécuritaires: Proceedings of the ICOLD 2019 Symposium,(ICOLD 2019), June 9-14, 2019, Ottawa, Canada/Publications du symposium CIGB 2019, juin 9-14, 2019, Ottawa, Canada. CRC Press, p. 47.

Montazerin, N., Akbari, G., Mahmoodi, M., 2015. Developments in turbomachinery flow: Forward curved centrifugal fans. Woodhead Publishing.

Mungkasi, S., Roberts, S.G., 2010. A new analytical solution for testing debris avalanche numerical models. ANZIAM Journal 52, 349-363.

Novák, P., Moffat, A., Nalluri, C., Narayanan, R., 2007. Hydraulic structures. CRC Press.

Ozmen-Cagatay, H., Kocaman, S., 2010. Dam-break flows during initial stage using SWE and RANS approaches. Journal of Hydraulic Research 48, 603-611.

Ozmen-Cagatay, H., Kocaman, S., Guzel, H., 2014. Investigation of dam-break flood waves in a dry channel with a hump. Journal of Hydro-environment Research 8, 304-315.

Plate, E.J., 2002. Flood risk and flood management. Journal of Hydrology 267, 2-11.

Quecedo, M., Pastor, M., Herreros, M., Merodo, J.F., Zhang, Q., 2005. Comparison of two mathematical models for solving the dam break problem using the FEM method. Computer Methods in Applied Mechanics and Engineering 194, 3984-4005.

Ritter, A., 1892. Die fortpflanzung der wasserwellen. Zeitschrift des Vereines Deutscher Ingenieure 36, 947-954.

Rusche, H., 2002. Computational fluid dynamics of dispersed two-phase flows at high phase fractions. University of London.

Schmidgall, T., Strange, J., 1960. Floods resulting from suddenly breached dams. Miscellaneous Paper, 2-374.

Shaheed, R., Mohammadian, A., Gildeh, H.K., 2019. A comparison of standard k–ε and realizable k–ε turbulence models in curved and confluent channels. Environmental Fluid Mechanics 19, 543-568.

Shigematsu, T., Liu, P.L.-F., Oda, K., 2004. Numerical modeling of the initial stages of dam-break waves. Journal of Hydraulic Research 42, 183-195.

Shih, T.-H., Liou, W.W., Shabbir, A., Yang, Z., Zhu, J., 1995. A new k-ϵ eddy viscosity model for high reynolds number turbulent flows. Computers & fluids 24, 227-238.

Shirkhani, H., Mohammadian, A., Seidou, O., Kurganov, A., 2016. A well-balanced positivity-preserving central-upwind scheme for shallow water equations on unstructured quadrilateral grids. Computers & Fluids 126, 25-40.

Smagorinsky, J., 1963. General circulation experiments with the primitive equations: I. The basic experiment. Monthly weather review 91, 99-164.

622 Stansby, P., Chegini, A., Barnes, T., 1998. The initial stages of dam-break flow. Journal of Fluid
623 Mechanics 374, 407-424.
624
625 Stoker, J., 1957. Water waves Interscience Publishers. Inc, New York.
626
627 Taheri, M., Dolatabadi, N., Nasseri, M., Zahraie, B., Amini, Y., & Schoups, G. (2020). Localized
628 linear regression methods for estimating monthly precipitation grids using elevation, rain gauge,
629 and TRMM data. Theoretical and Applied Climatology, 142(1), 623-641.
630
631 Tajnesaie, M., Jafari Nodoushan, E., Barati, R., Azhdary Moghadam, M., 2020. Performance
632 comparison of four turbulence models for modeling of secondary flow cells in simple trapezoidal
633 channels. ISH Journal of Hydraulic Engineering 26, 187-197.
634
635 Taylor, K.E., 2001. Summarizing multiple aspects of model performance in a single diagram.
636 Journal of Geophysical Research: Atmospheres 106, 7183-7192.
637
638 Van Emelen, S., Zech, Y., Soares Frazao, S., 2014. Limitations of the shallow water assumptions
639 for problems involving steep slopes: Application to a dike overtopping test case, River flow
640 2014.
641
642 Vosoughi, F., Rakhshandehroo, G., Nikoo, M.R., Sadegh, M., 2020. Experimental study and
643 numerical verification of silted-up dam break. Journal of Hydrology 590, 125267.
644
645 Wang, B., Chen, Y., Peng, Y., Zhang, J., Guo, Y., 2020a. Analytical Solution of Shallow Water
646 Equations for Ideal Dam-Break Flood along a Wet-Bed Slope. Journal of Hydraulic Engineering
647 146, 06019020.
648
649 Wang, B., Chen, Y., Wu, C., Peng, Y., Song, J., Liu, W., Liu, X., 2018. Empirical and semi-
650 analytical models for predicting peak outflows caused by embankment dam failures. Journal of
651 Hydrology 562, 692-702.
652

Wang, B., Liu, W., Zhang, J., Chen, Y., Wu, C., Peng, Y., Wu, Z., Liu, X., Yang, S., 2020b. Enhancement of semi-theoretical models for predicting peak discharges in breached embankment dams. Environmental Fluid Mechanics, 1-20.

Wang, J.S., Ni, H.-G., He, Y.-S., 2000. Finite-difference TVD scheme for computation of dam-break problems. Journal of Hydraulic Engineering 126, 253-262.

Wang, W., Wang, M., 2011. Application of KE Model on the Numerical Simulation of a Semi-confined Slot Turbulent Impinging Jet, 2011 Fourth International Joint Conference on Computational Sciences and Optimization. IEEE, pp. 86-89.

Weller, H.G., Tabor, G., Jasak, H., Fureby, C., 1998. A tensorial approach to computational continuum mechanics using object-oriented techniques. Computers in physics 12, 620-631.

Wood, A., Wang, K.-H., 2015. Modeling dam-break flows in channels with 90 degree bend using an alternating-direction implicit based curvilinear hydrodynamic solver. Computers & Fluids 114, 254-264.

Wu, W., Wang, S.S., 2007. One-dimensional modeling of dam-break flow over movable beds. Journal of hydraulic engineering 133, 48-58.

Yan, X., Mohammadian, A., Rennie, C.D., 2020. Numerical modeling of local scour due to submerged wall jets using a strict vertex-based, terrain conformal, moving-mesh technique in OpenFOAM. International Journal of Sediment Research.

Yang, X., Xu, W.-l., Luo, S.-j., Chen, H.-y., Li, N.-w., Xu, L.-j., 2011. Experimental study of dam-break flow in cascade reservoirs with steep bottom slope. Journal of Hydrodynamics, Ser. B 23, 491-497.